Influence of Y_2BaCuO_5 particles on the microstructure of $YBa_2Cu_3O_{7-x}$ (123)-Y_2BaCuO_5 (211) melt-textured superconductors

Pavel Diko
Institute of Experimental Physics, Slovak Academy of Sciences, Watsonova 47, 04353 Kosice, Slovakia

Wolfgang Gawalek, Tobias Habisreuther, Thomas Klupsch, and Peter Görnert
Institut für Physikalische Hochtechnologie, Helmholtzweg 4, 100239 Jena, D-07702, Germany
(Received 30 June 1995)

The paper is devoted to the microstructural defects in melt-processed YBaCuO which can be active either as magnetic-flux-pinning centers or weak links. The influence of 211 particles in 123-211 melt-textured bulk superconductors on the microstructural features such as microcracking, subgrains, twins, and twin complexes was studied by polarized light microscopy. The observed linear dependence between *a-b* microcrack spacing, and l_c, and $d_{211} \cdot V_{123}/V_{211}$ (d_{211} means 211 particle size, V_{123} means 123 volume fraction, V_{211} means 211 volume fraction) proves that the microcracking process can be described under the framework of a model devised for the multiple failure of a unidirectional composite under uniaxial tensile loading. Shorter mean-free distance between 211 particles depresses the subgrain thickness, the twin complex size, and twin spacing. The level of residual tensile stress in the 123 *a-b* plane was estimated from detwinning observed around 211 particles.

I. INTRODUCTION

Melt texturing is the most promising method for producing bulk-type 123 superconductors.[1,2] This technique involves heating the material above the peritectic temperature followed by a slow cooling to allow directional growth of 123 domains. The bulk superconductor obtained is a composite of the 123 phase matrix with 211 nonsuperconducting particles.

Although the relatively large J_c values indicate the existence of effective flux-pinning mechanisms in the melt-textured 123, the exact pinning mechanisms are still unclear The intrinsic weakly superconducting layers of 123 were suggested to be natural pinning sites.[4] In addition, defects such as twin planes,[5] stacking faults,[6,7] dislocations,[8] oxygen-deficient regions,[9] and 211 particles[10] have been proposed to act as pinning centers. Even though experimental evidenced suggests that these defects may serve as pinning sites, their effectiveness in pinning and the proportion of their contribution to the measured J_c values are as yet not established.

It seems that superconducting properties can be optimized mainly by controlling the volume fraction and particle size of the 211 phase. This phase has an essential influence on the crystal and microstructural defects in melt-textured 123 superconductors. The volume fraction and the size of 211 particles can be influenced by the heat treatment profile,[3,12] by excess of Y in nominal composition and by Pt (Ref. 12) or Ce (Ref. 13) additions.

The microstructural features of these composites have been intensively studied. The lines parallel with the *a-b* plane, which have been observed in the microgrpahs, are commonly considered to be low-angle grain boundaries[3,14–17] or defects formed due to the highly anisotropic nature of growth resulting in the formation of gaps filled with rejected liquid phase between the platelets.[4,18–20] Jin[15] found that the spacing of these lines l_c is linearly dependent on the 211 particle size. According to McGinn *et al.*,[17] an increase in the volume fraction of 211 results in the decrease of platelet thickness.

The cracks found parallel to the *a-b* planes are usually ascribed to the cracking due to expansion anisotropy[21] (thermal stress gradients) along low-cohesion low-angle boundaries between platelet grains[14] or due to the presence of CuO and Ba-cuprate phases between platelet grains.[16] Other results emphasize the essential role of 211 particles in the microcracking process allowing fast oxygenation, the introduction of inhomogeneous residual stresses, and the refinement of twin spacing.[22]

The aim of this paper is to describe the relationship between 211 particles and defects such as microcracks, twins, and subgrains. As a basic method, polarized microscopy is used. Its advantage follows from the high optical anisotropy of layered cuprates which allows the visualization of microstructural details which are not seen by scanning electron microscopy.

II. EXPERIMENTAL

In the present study, the well textured bulk $YBa_2Cu_3O_{7-x}$ samples, with different 211 volume fraction and size, were prepared by a melt-texturing process at IPHT Jena. The microstructure was analyzed mainly by optical microscopy (Neophot 21) after polishing or etching in a solution of bromine in ethanol (2 wt. % Br). Observation in normal and polarized light was performed. The position of the polarizers is indicated in the micrographs. The orientation of 123 grains was determined form their optical twin patterns.[23] The declination angle α is then defined as the angle between the normal to the polished surface and the [001] direction.

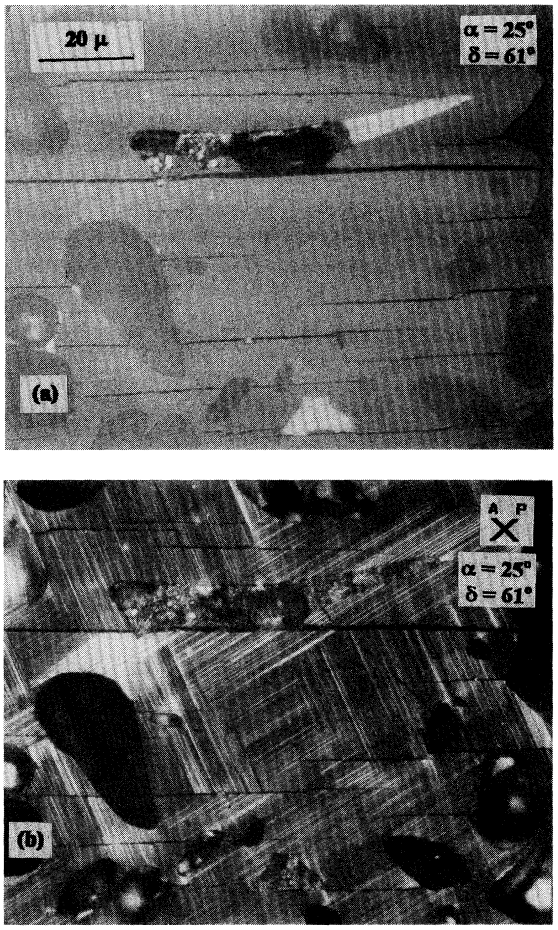

FIG. 1. Growth related a-b planar defect [filled with CuO (white) and BaCuO] and a-b microcracks. Image in normal light (a). Twin matching across the a-b microcracks. Polarized light (b).

The definition of angle δ is according to Verhoeven and Gibson.[23]

The volume fraction of 211 phase (V_{211}) was measured by the point counting method. The size of 211 particles (d_{211}) represents the mean longest dimension of the 211 particle on the polished surface. The size of twin complexes, spacing of twins and a-b microcracks, and the number of 211 particles per unit length (N_{211}) were measured by the linear intercept method.[24] The mean-free distance between 211 particles (MFD_{211}) was calculated using

$$\mathrm{MFD}=\frac{1-V_{211}}{N_{211}}. \tag{1}$$

Scanning electron microscopy with energy dispersive x-ray microanalysis was also used for a comparative study with optical microscopy.

III. RESULTS AND DISCUSSION

A. Microcracking in a-b plane and growth related a-b planar defects

The first aim of this investigation was to distinguish between the a-b microcracks formed in solid state and the a-b planar defects formed during the crystallization process according to the models proposed by Alexander *et al.*[18] and Goyal *et al.*[20] In the samples that were studied, it was found that some growth related a-b planar defects exist [Figs. 1(a) and 1(b)]. They are filled with rejected liquid (CuO, Ba-Cu-O) and are clearly distinguishable from the a-b cracks. Their tips are oval due to sufficiently fast diffusion of cations at the crystallization temperatures. Such growth related a-b planar defects were observed in the samples with large 211 particles but they account for less than 1% of all a-b planar defects. The remaining a-b planar defects are microcracks formed mainly at the transition from the tetragonal to orthorhombic phase.[22] They are formed due to the higher thermal expansion of the 123 phase compared to the 211 phase[21] and also because the fracture toughness of the orthorhombic 123 $K_c(100)<K_c(010)\gg K_c(001)$.[25] The difference in thermal expansion introduces tensile stresses into the 123 matrix and compressive stresses into the 211 particles.

It is often emphasized that in 123-211 melt-textured samples with a small 211 particle size, a-b planar defects (in fact microcracks) do not exist.[16] Analysis of samples in the as-polished condition, with mean particle size close to 2 μm shows little evidence of any a-b microcracks (Fig. 2). After etching, the a-b microcracks appear to be associated with very fine 211 particles (Fig. 3). Visualization of a-b microcracks also in the samples with very small 211 particles, allows the measurement of the crack spacing l_c in a broad range of mean 211 particle size d_{211} and 211 volume fraction V_{211}. The true microcrack spacing was obtained knowing crystal orientation determined from its optical twin pattern.[23] When l_c is plotted versus $(d_{211}\cdot V_{123})/V_{211}$ the linear dependence appears with some deviation for the smallest particles (Fig. 4).

The observed linear dependence between l_c and $(d_{211}\cdot V_{123})/V_{211}$ proved that the microcracking process in 123-211 composites can be described in the framework of the model devised for the multiple failure of a unidirectional composite under uniaxial tensile loading.[26] For such a case the crack spacing l_c is given by

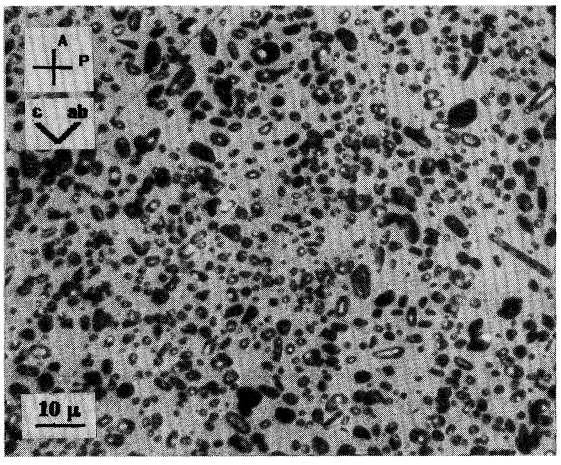

FIG. 2. Microcracks are not visible after polishing of the sample with small 211 particles.

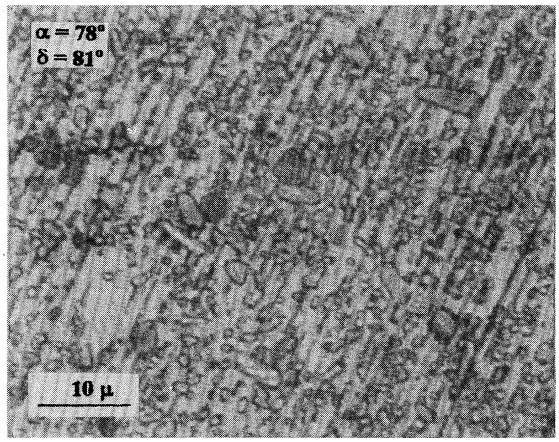

FIG. 3. *a-b* microcracks visualized by etching.

$$l_c = \frac{\sigma_m^* \cdot r V_m}{2 \tau V_f}, \tag{2}$$

where r is the fiber radius (211 particle size in this case), σ_m^* is the tensile strength of matrix (in this case the maximum tensile stress that can be applied to the 123 phase, i.e., tensile fracture strength), τ is either the frictional stress (unbonded case) or the maximal shear stress (bonded case) between fibers and matrix (here the 211-123 interface), V_m and V_f are the volume fractions of matrix and fibers, respectively (here the 123 and 211 volume fractions). In this case the 211 particles are under compression so they are not cracked. The 123 phase can be considered as the matrix between 211 particles and it is under tensile stress in the "c" direction. The multiple matrix cracking by no means implies complete unloading of the matrix.[26] The maximum residual tensile stresses in the c direction were estimated[22] to be 290 MPa.

The constant ratio between tensile strength of 123 matrix (σ_m^*) and the maximum shear stress (τ) can be deduced from the linear dependence between l_c and $d_{211} \cdot V_{123}/V_{211}$.

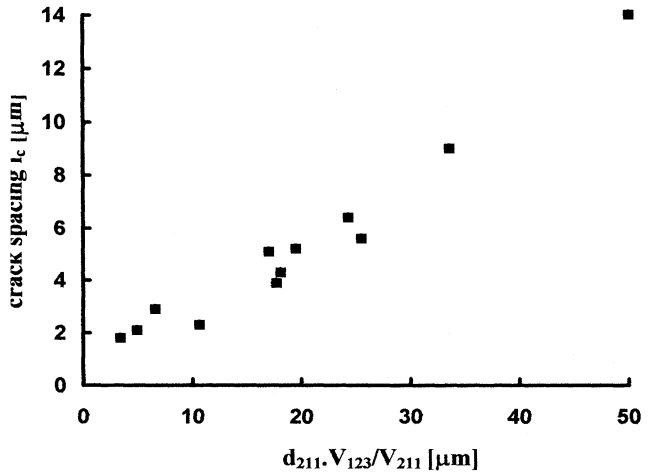

FIG. 4. Dependence between the crack spacing l_c and $d_{211} \cdot V_{123}/V_{211}$.

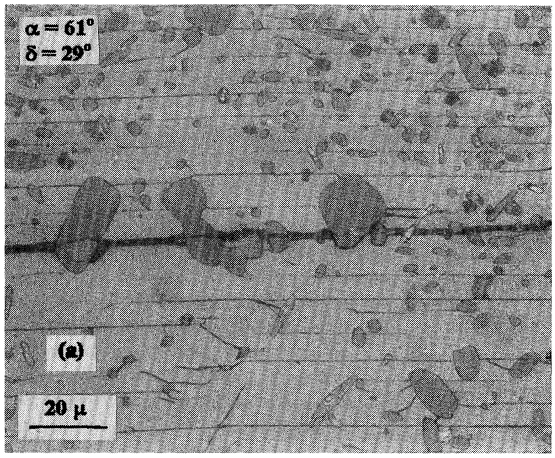

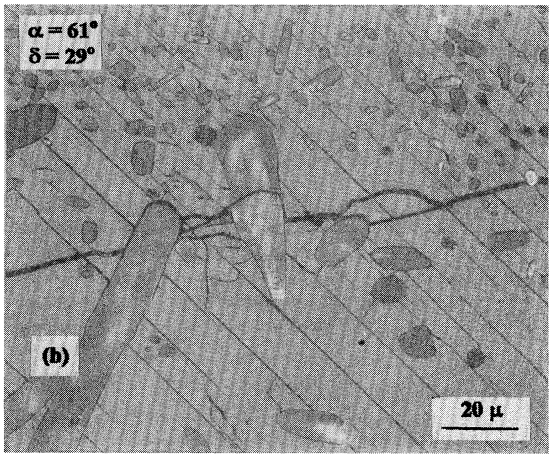

FIG. 5. *a-b* macrocrack (a) and random macrocrack (b) propagating across 211 particles and delaminating the 211/123 interface.

This also means that, in the entire measured range of d_{211}, the 123-211 interface does not fail by microcracking.

The deviation from the linear dependence between l_c and $d_{211} \cdot V_{123}/V_{211}$ may be associated with the existence of a critical 211 particle size below which spontaneous cracking does not occur. This critical size effect was proposed to be a result of elastic stored energy of the misfit particle being proportional to its volume, while the crack resistance force is related to its area.[27] For 123-211 composite this critical particle size is below 1 μm. The 211 particles smaller than critical will lead to higher residual stresses which can be relaxed only by plastic deformation processes. This could explain the higher density of dislocations at the near smaller 211 particles observed by Mironova, Lee, and Salama.[28]

At a collision of the 211 particle with a macrocrack, it can be cross cracked [Figs. 5(a) and 5(b)]. Macrocracks are created in multidomain bulk 123-211 composites under the influence of stresses arising at cooling due to the anisotropy of the 123 phase thermal expansion[20] or due to the difference in thermal expansion of 123 and larger secondary phase islands.[22] The microcracks are usually parallel to the *a-b* plane [Fig. 5(a)] but can sometimes take random orientation [Fig. 5(b)].

The influence of microcracking on the pinning of flux

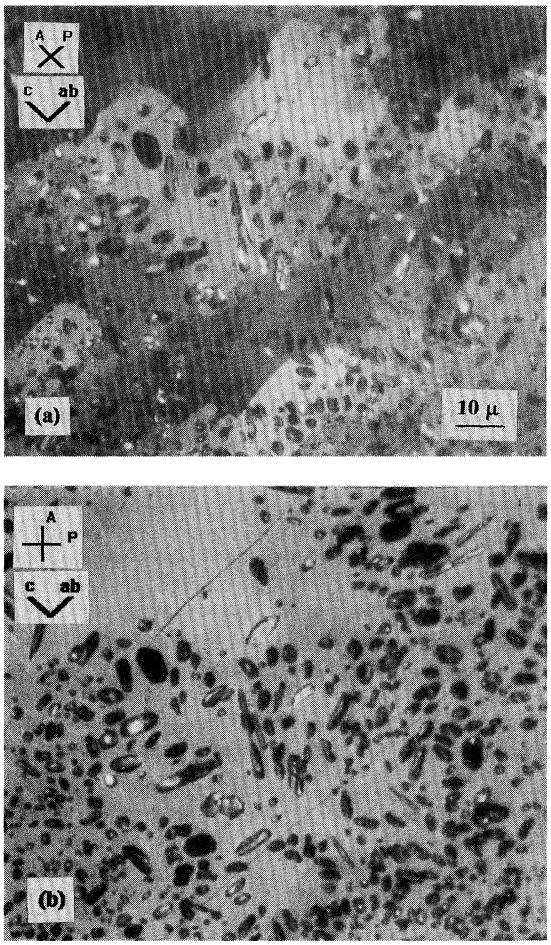

FIG. 6. Subgrains (a) in the sample with small 211 particles (b).

lines has not been considered so far. The surface area per unit volume is comparable with that of 211 particles, therefore they can also contribute to the pinning process. It is possible to expect the attraction of flux lines by the surface of microcracks. This interaction could be analyzed in a similar way as it was done for the interaction between 211 particles and the 123 phase by Murakami.[10] The pinning force should be strongly anisotropic having a maximum for the flux lines parallel to the crack surface moving perpendicularly to the crack surface.

B. Subgrains

If a 123 grain is in a suitable orientation, subgrains can be visible in polarized light [Figs. 6(a), 6(b), and 7]. Such a condition arises when the c axis is lying in the sample surface and is oriented nearly parallel or perpendicular to the light polarization vector (extinction position). In such a way the crystal misorientation of some degrees is revealed. The explanation as to why subgrains are visualized at their special orientation to the light polarization vector can be related to the fact that only tilting of the c axis (without the rotation around it) occurs in the subgrain formation. Such a tilting enables visualization of the subgrains in the planes parallel to the c direction because only subgrains having their c axis

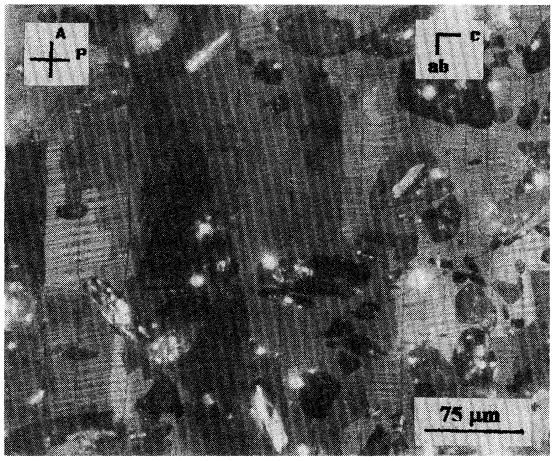

FIG. 7. Subgrains in the sample with large 211 particles.

parallel (or perpendicular) to the light polarization vector are dark (in extinction). The brightness of other subgrains depends on their tilting from the extinction orientation. In the a-b plane, the contribution of c-axis tilting to the changes in intensity of reflected light during a-b plane rotation is not high enough to visualize the subgrains. In the a-b plane, this effect is also shadowed by the contrast from twin complexes which has its maximum when the a-b plane is perpendicular to the incident polarized light.

The subgrains have an approximately rectangular shape with segments of boundaries parallel or perpendicular to the a-b plane. It should be noted that the subgrain boundaries are not cracked and no secondary phase appears in them (Fig. 6). As the cross-section plane in Figs. 6 and 7 is almost parallel to the a-c and b-c planes, the thickness of the subgrains l_s can be measured directly. The mean-free distance between 211 particles (MFD_{211}) does not have a great influence on the subgrain thickness l_s. The subgrain thickness is approximately 25 μm for the sample with $MFD_{211}=50$ μm (Fig. 7), and 12 μm for the sample with $MFD_{211}=3$ μm [Fig. 6(a)].

Taking into account the dimensions of the observed subgrains, we can relate their origin to the crystallization process rather than to some polygonization processes in the solid state.[29] The tilting angle θ has maximum at about 5–6° so boundaries between subgrains are of low-angle type.[22] Low-angle boundaries between subgrains should be formed by walls of dislocations with the Burgers vectors b of $\langle 100\rangle$,$\langle 110\rangle$ or $\langle 001\rangle$ types and with a spacing $d=b/\theta$. Since the dislocation core diameter is about 1 nm, only at misorientation angles higher than 11° do the dislocations act as weak links.[30] At lower angles these dislocations will act as pinning centers.

C. Twins and twin complexes

1. Twins

The twinning of the 123 phase, with the (110) and $(1\bar{1}0)$ twinning planes, occurs at its transformation from the tetragonal to orthorhombic state.[31,32] The twin spacing l_t depends on the local microstructure. Generally, l_t is higher in regions

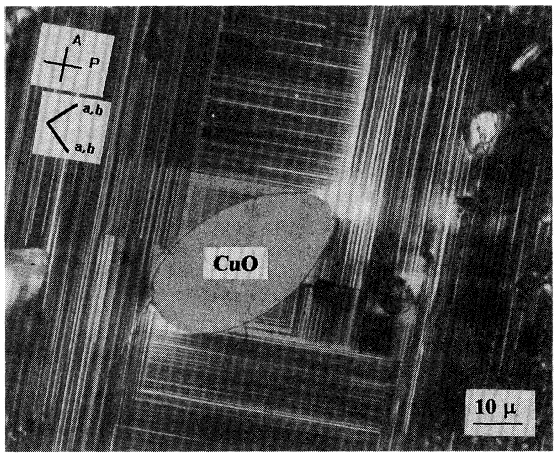

FIG. 8. Detwinning areas and areas with predominant one twin domain variant extended in the ⟨100⟩ directions around CuO and 211 particles.

with a lower concentration of 211 particles (Figs. 8 and 9). The relationship between l_t and the crystal dimension can be expressed as[33]

$$l_t=(g\gamma/CMF2)^{1/2}, \tag{3}$$

where $F=2(b-a)/(a+b)$ is the orthorhombicity and g and M are the grain size and the shear modulus, respectively. C is a constant nearly equal to 1 and γ is the twin boundary energy. The validity of this relationship was also tested for thin films but for thin films, the critical length is the thickness of the film rather than the grain size.[34]

In the case of 123-211 composite the effective dimension factor at the twin nucleation can be either the a-b microcrack spacing or the local effective MFD_{211}. The question is whether the a-b cracks are present before the twin formation. It was shown that the tetragonal-orthorhombic (T-O) transformation is a multistep transformation.[35,36] First, a so-called tweed orthorhombic structure is formed (pseudotetragonal), consisting of orthorhombic clusters on a 10 nm scale. In this state the ordering of oxygen in the a-b planes can cause hardening leading to a decrease in the fracture toughness in

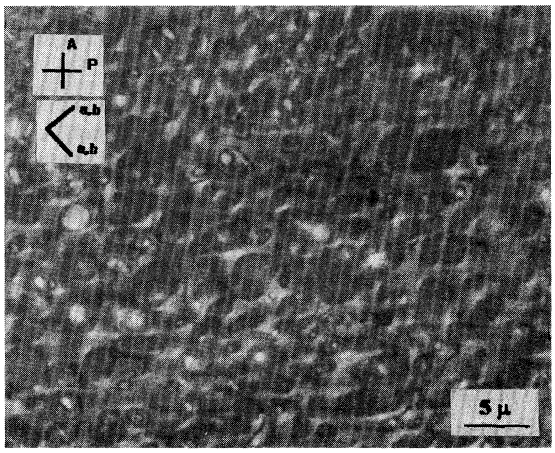

FIG. 9. Detwinning areas around small 211 particles.

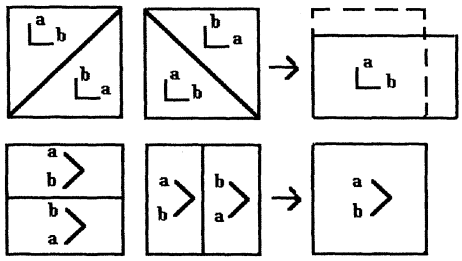

FIG. 10. Plastic strain in the ⟨100⟩ and ⟨110⟩ directions associated with the detwinning process.

these planes resulting in a-b crack formation. Only in the next step is the twin structure formed. However, detailed study of a twin structure [Fig. 1(b)] often shows an excellent twin matching across the a-b microcracks. This means that the effective dimension factor during the twin formation was larger than final crack spacing or, in other words, the microcracks are mainly formed during cooling down from the T-O transformation temperature. This is also evidence supporting the idea that the observed planar defects in melt-textured 123 are microcracks formed when the crystallization process is finished. From such a consideration it can be concluded that it is mainly the mean-free distance between 211 particles (MFD_{211}), as a characteristic dimension, that determines the twin spacing l_t. According to Eq. (2) it is therefore reasonable to expect the twin spacing l_t will have a square-root dependence on MFD_{211}. This is difficult to test form the micrographs taken by optical microscopy because, at lower MFD_{211}, the twin spacing l_t is well under the resolution limit of optical microscopy.

An interesting feature observed in melt-textured samples was detwinning around 211 particles and secondary phases. In Figs. 3 and 4 the detwinning areas, or areas with predominant one twin domain variant, developed around CuO particles and around 211 particles. These areas extend in the ⟨100⟩ directions forming a rosette. It is believed that they were formed by twin boundary motion. Twin boundary motion partially relaxes the tensile stresses around CuO and 211 particles created at cooling due to lower thermal expansion of the 211 and CuO phases than the 123 matrix.

Closer analysis shows that simple motion of twin boundaries is not sufficient to cause the relaxation of stresses around a 211 particle in all directions lying in the a-b plane. The drawings in Fig. 10 confirm the dimension changes due to diminishing of one twin type. Clearly, normal stresses perpendicular and parallel to the twin boundaries do not relax by the twin boundary motion. So in the ⟨110⟩ directions the twinning structure does not change by thermal stresses around 211 and CuO particles.

The detwinning process due to the stresses around the 211 particles leads to the high inhomogeneity of twins and twin spacing in the samples with higher 211 volume fraction and finer particle size (Fig. 9) These regions appear as shadows and bright fields extended around the 211 particles in the ⟨100⟩ directions.

The motion of twin boundaries indicates that residual tensile stresses exist in the a-b plane at a level that is necessary for the detwinning process. The stress necessary for the twin boundary motion has been theoretically estimated[37] to be in

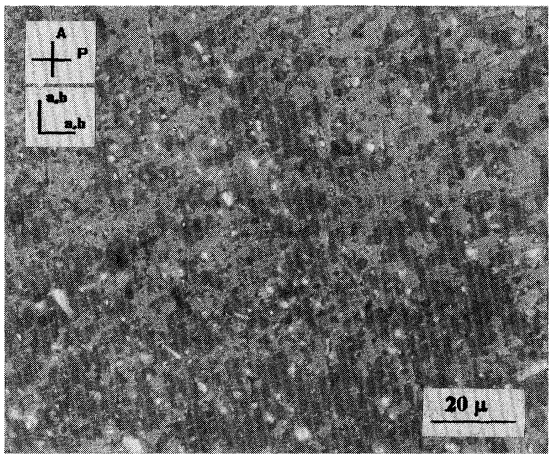

FIG. 11. Twin complexes visualized in polarized light.

the range of 130–400 MPa which is in agreement with experimental determinations[38–40] carried out at 350 °C (50–100 MPa).

The stresses arising due to the 123-211 difference in expansion can contribute to flux pinning. They can cause the crystal defect formation (dislocations stacking faults) around the 211 particles and can influence the twin structure both during and after a *T-O* transformation. Since residual stresses are highly inhomogeneous, they will lead to the local fluctuations of T_c.[41,42]

2. *Twin complexes*

A lamellar assembly of twins with parallel (110) or ($1\bar{1}0$) walls (twin complexes) can be visualized[43] under slightly uncrossed polarizers when polarizer and analyzer are nearly parallel or perpendicular to the *a* and *b* directions[44] (Fig. 10). Contrast between twin complexes is highest in the *a-b* plane and disappears when the *c* axis lies in the surface. Twin complexes are visualized due to the higher optical conductivity for light impinging with the light polarization vector parallel to the twin walls than for the light polarization vector perpendicular to the walls.[44]

The twin complex boundaries prefer the orientation parallel to (110) and ($1\bar{1}0$) planes (Fig. 11). The mean linear size of the twin complexes l_{tc} in the samples with different mean-free distance between 211 particles (MFD_{211}) was measured by the linear intercept method. The results summarized in Table I, show that l_{tc} is essentially depressed by lowering MFD_{211}.

The twin complex boundaries are places of higher distortion of 123 lattice and therefore they can also contribute to the pinning of flux lines. Their contribution to the critical current density can be treated similarly as in the work of Kes *et al.*[5]

TABLE I. Measured values of 211 volume fraction V_{211} mean-free distance between 211 particles MFD_{211} and mean twin complex size l_{tc}.

Sample	V_{211}	MFD_{211} (μm)	l_{tc} (μm)
1	0.36	50	25
2	0.32	12	8
3	0.29	7.3	4.5

IV. CONCLUSIONS

(i) It has been shown that the *a-b* microcracks can be clearly visible after etching the 123-211 samples with the 211 particle size close to 1 μm. The microcracks are easily distinguishable from *a-b* growth related planar defects. The growth related *a-b* planar defects account for less than 1% of all *a-b* planar defects. *a-b* planar defects in the melt-processed Y-Ba-Cu-O superconductors are mainly microcracks formed preferentially in the orthorhombic 123 phase due to the lower thermal expansion of 211 than that of the 123 phase.

(ii) The observed linear dependence between microcrack spacing l_c and $d_{211} \cdot V_{123}/V_{211}$ (d_{211} means 211 particle size, V_{123} means 123 volume fraction, and V_{211} means 211 volume fraction) proves that the microcracking process in melt-textured 123-211 can be described under the framework of a model devised for the multiple failure of a unidirectional composite under uniaxial tensile loading. The constant ratio between tensile strength of 123 matrix (σ_m^*) and the maximum shear stress (τ) can be deduced from the linear dependence between l_c and $d_{211} \cdot V_{123}/V_{211}$. This also means that, in the whole measured range of d_{211}, the 123-211 interface does not fail by microcracking.

(iii) Other observed types of crystal defects are subgrain boundaries. The subgrain boundaries are not cracked and no secondary phases appear on them. The subgrains are visible in polarized light when the *c* axis is lying in the sample surface and is oriented nearly parallel or perpendicularly to the light polarization vector (extinction position). The subgrain thickness was not found to be strongly influenced by the mean-free distance between 211 particles (MDE_{211}).

(iv) The twin structure is refined by 211 particles. A square-root dependence of twin spacing on the mean-free distance tween 211 particles MFD_{211} was deduced.

(v) The twin complex size was found strong depressed by shortening the mean-free distance between 211 particles (MDF_{211}).

(vi) Areas, with one predominant twin-type variant, extended around 211 particles in ⟨110⟩ directions, are formed by the twin motion under stresses arisen due to lower thermal expansion of 123 than 211 phase. The twin boundary motion proves that residual tensile stresses (of around 50–100 MPa) exist in the *a-b* plane.

(vii) The microcracks, subgrain boundaries twin complex boundaries, twins, and inhomogeneous tensile stresses around 211 particles can contribute to the flux-line pinning in Y-Ba-Cu-O melt-textured superconductors. Their density can be increased by higher volume fraction and refinement of 211 particles.

ACKNOWLEDGMENTS

This work has been supported by the Grant Agency of Slovak Academy of Sciences (Project No.1 2/1323/94) and by the Deutsche Forschungsgemeinschaft (Project YBCO-HRPLM).

[1] S. Jin, T. Tiefel, R. Sherwood, R. van Dover, M. Davis, G. Kamlot, and R. Fastnacht, Phys. Rev. B **37**, (1988).
[2] M. Murakami, M. Morita, K. Doi, and K. Miyamoto, Jpn. J. Appl. Phys. **28**, 1189 (1989).
[3] K. Salama, V. Selvamanickam, L. Gao, and K. Sun, Appl. Phys. Lett. **54**, 2352 (1989).
[4] M. Tachiki and S. Takahashi, Solid State Commun. **70**, 291 (1989).
[5] S. Kes, A. Pruymboom, J. van der Berg, and J. A. Mydosh, Cryogenics, **29**, 228 (1989).
[6] K. Yamaguchy, M. Murakami, H. Fujimoto, S. Gotoh, Y. Shiohara, N. Koshizuka, and S. Tanaka, J. Mater. Res. **6**, 1404 (1991).
[7] R. Ramesh, S. Jin, S. Nakahara, and T. H. Tiefel, Appl. Phys. Lett. **57**, 1458 (1990).
[8] V. Selvamanickam, M. Mironova, S. Son, and K. Salama, Physica C **208**, 238 (1993).
[9] M. Dauemling, J. M. Seuntjens, and D. C. Larbalestier, Nature (London) **346**, 332 (1990).
[10] M. Murakami, S. Gotoh, H. Fujimoto, K. Yamaguchi, N. Koshizuka, and S. Tanaka, Supercond. Sci. Technol. **4**, S43 (1991).
[11] J. Ringnalda, X. Yao, D. G. McCartney, C. J. Kiely, and G. J. Tatlock, Mater. Lett. **13**, 357 (1992).
[12] N. Ogava, I. Hirabayashi, and S. Tanaka, Physica C **177**, 101 (1991).
[13] C. J. Kim, S. H. Lai, and P. J. McGinn, Mater. Lett. **19**, 185 (1994).
[14] A. Goyal, P. D. Funkenbusch, D. M. Kroeger, and S. J. Burns, Physica C **182**, 203 (1991).
[15] S. Jin, G. W. Kammlott, T. H. Tiefel, T. T. Kodas, T. L. Ward, and D. M. Kroeger, Physica C **181**, 57 (1991).
[16] R. L. Meng, Y. Y. Sun, P. H. Hor, and C. W. Chu, Physica C **179**, 149 (1991).
[17] P. McGinn, W. Chen, N. Zhu, M. Lanagan, and U. Balachandran, Appl. Phys. Lett. **57**, 1455 (1990).
[18] K. B. Alexander, A. Goyal, D. M. Kroeger, V. Selvamanickam, and K. Salama, Phys. Rev. B **45**, 5622 (1992).
[19] T. Izumi and Y. Shiohara, J. Mater. Res. **7**, 16 (1992).
[20] A. Goyal, K. B. Alexander, D. M. Kroeger, P. D. Funkenbusch, and S. J. Burns, Physica C **210**, 197 (1993).
[21] A. Goyal, W. C. Oliver, P. H. Funkenbusch, D. M. Kroeger, and S. J. Burns, Physica C **183**, 221 (1991).
[22] P. Diko, N. Pelerin, and P. Odier, Physica C **243**, 169 (1995).
[23] J. D. Verhoeven and E. D. Gibson, Appl. Phys. Lett. **52**, 1190 (1988).
[24] J. H. Richardson, *Optical Microscopy for the Materials Science* (Dekker, New York, 1971), p. 599.
[25] A. S. Raynes, S. W. Freiman, F. W. Gayle, and D. L. Kaiser, J. Appl. Phys. **70**, 5254 (1991).
[26] S. Y. Zhang, in *Handbook of Ceramic and Composites*, edited by Nicholas P. Cheremisonof (Dekker, New York, 1992), Vol. 2, p. 56.
[27] R. W. Davidge and T. J. Green, J. Mater. Sci. **3**, 629 (1968).
[28] M. Mironova, D. F. Lee, and K. Salama, Physica C **211**, 188 (1993).
[29] F. Sandjumenge, S. Pinol, X. Obradors, E. Snoek, and Ch. Roucau, Phys. Rev. B **50**, 7032 (1994).
[30] Y. Gao, K. L. Merkle, G. Bai, H. L. M. Chang, and D. J. Lam, Physica C **174**, 1 (1991).
[31] M. Hervieu, B. Domenges, C. Michel, G. Heger, J. Provost, and B. Raveau, Phys. Rev. B **36**, 3920 (1987).
[32] H. W. Zandbergen, G. Van Tendeloo, T. Okabe, and S. Amelinckx, Phys. Status Solidi **103**, 45 (1987).
[33] Y. Zhu, T. Tafto, and M. Suenaga, MRS Bull. **15**, 54 (1991).
[34] S. K. Streiffer, E. M. Zielinsky, B. M. Lairson, and J. C. Bravman, Appl. Phys. Lett. **58**, 2171 (1991).
[35] T. Icihashi, S. Iijima, Y. Kubo, Y. Shimankawa, and J. Tabuci, Jpn. J. Appl. Phys. **27**, L594 (1988).
[36] S. Semenovskaya and A. G. Khachaturyan, Phys. Rev. B **46**, 6511 (1992).
[37] D. Favrot, M. Dechamps, and A. Revcolevschi, Magn. Lett. **64**, 147 (1991).
[38] D. L. Kaiser, F. W. Gayle, R. S. Roth, and L. J. Swartzendruber, J. Mater. Res. **4**, 745 (1989).
[39] T. Hatanaka and A. Savada, Jpn. Appl. Phys. **28**, L794 (1989).
[40] H. Schmidt, E. Burkhard, B. N. Sun, and J. P. Rivera, Physica C **157**, 555 (1989).
[41] S. J. Burns, Supercond. Sci. Technol. **7**, 337 (1994).
[42] U. Welp, M. Grimsditch, S. Flescher, W. Nessler, B. Veal, and G. W. Crabtree, J. Supercond. **7**, 159 (1994).
[43] P. Diko, K. Csach, J. Miškuf, and V. Kavečanský, J. Mater. Sci. **24**, 1995 (1989).
[44] H. Rabe, J. P. Rivera, H. Schmid, J. P. Chaminade, and L. Naganga, Mater. Sci. Eng. **B5**, 243 (1990).

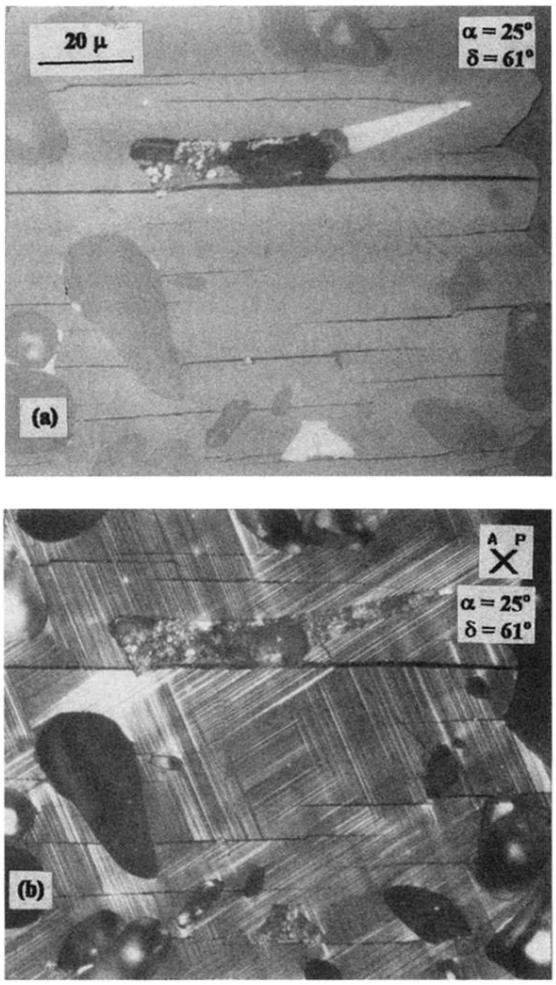

FIG. 1. Growth related *a*-*b* planar defect [filled with CuO (white) and BaCuO] and *a*-*b* microcracks. Image in normal light (a). Twin matching across the *a*-*b* microcracks. Polarized light (b).

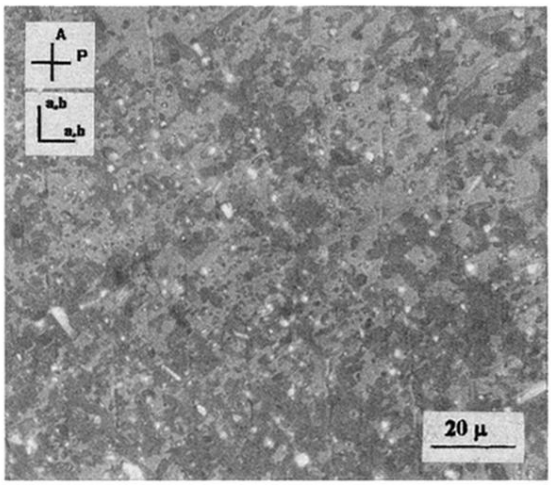

FIG. 11. Twin complexes visualized in polarized light.

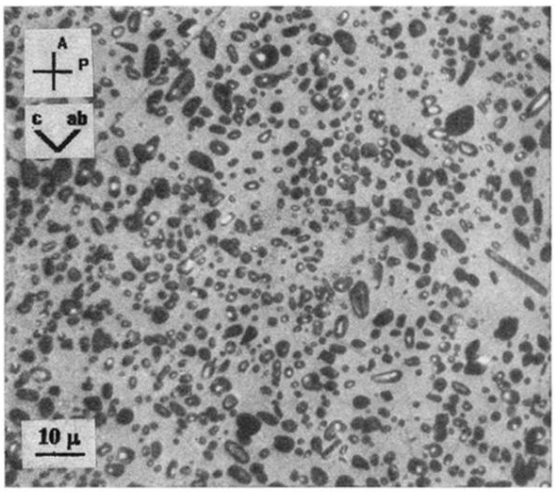

FIG. 2. Microcracks are not visible after polishing of the sample with small 211 particles.

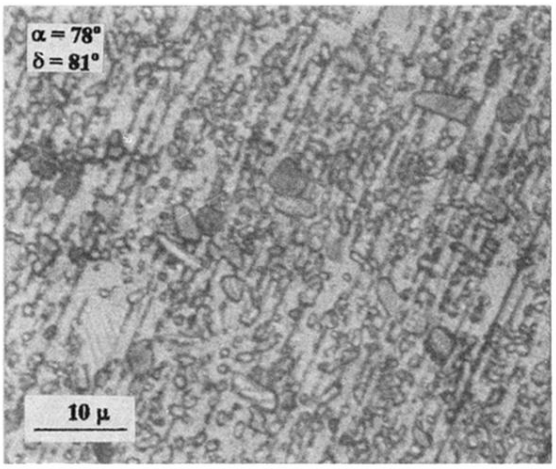

FIG. 3. *a*-*b* microcracks visualized by etching.

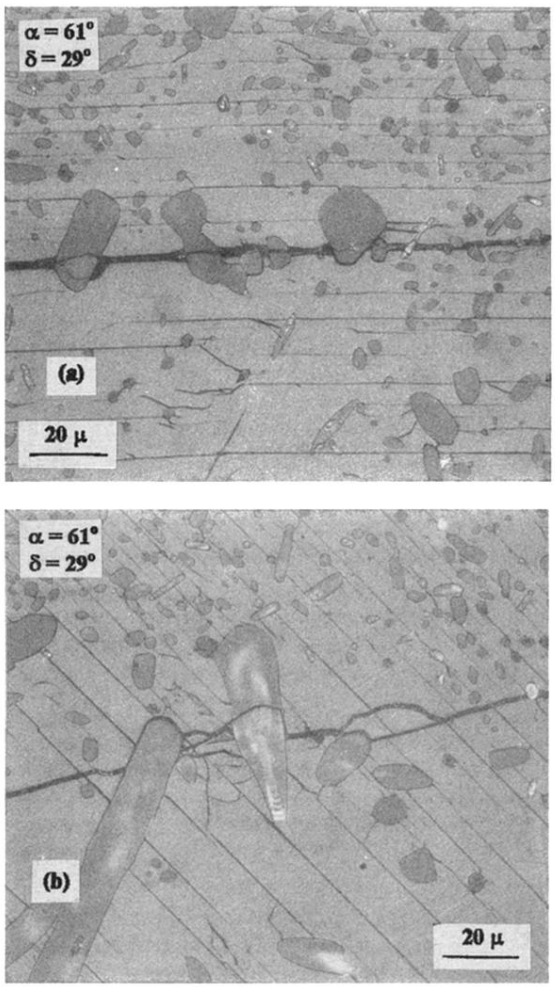

FIG. 5. *a-b* macrocrack (a) and random macrocrack (b) propagating across 211 particles and delaminating the 211/123 interface.

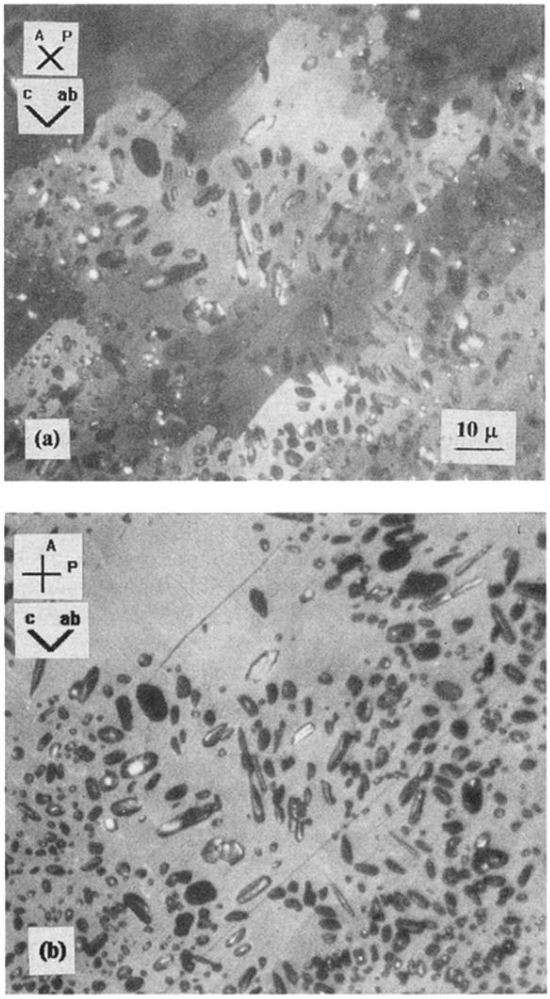

FIG. 6. Subgrains (a) in the sample with small 211 particles (b).

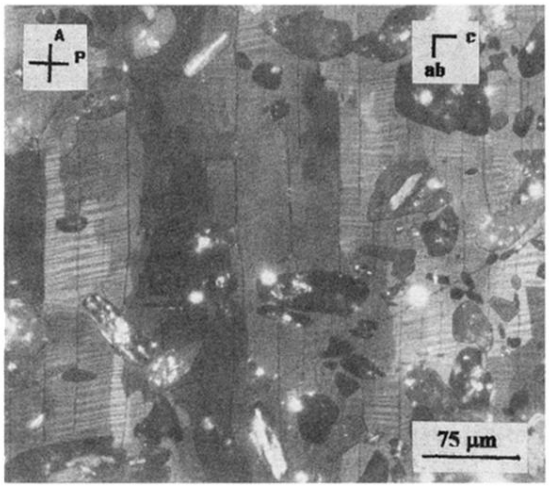

FIG. 7. Subgrains in the sample with large 211 particles.

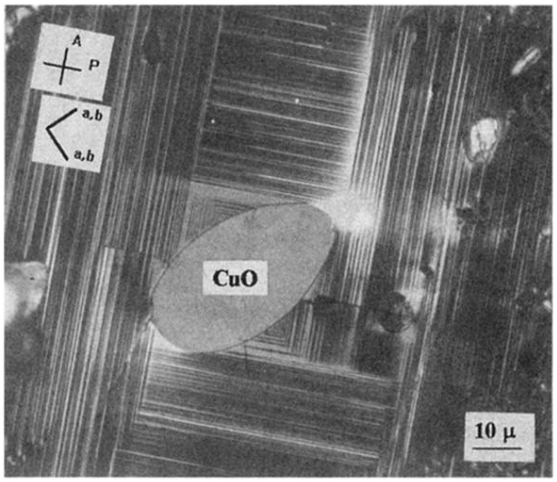

FIG. 8. Detwinning areas and areas with predominant one twin domain variant extended in the ⟨100⟩ directions around CuO and 211 particles.

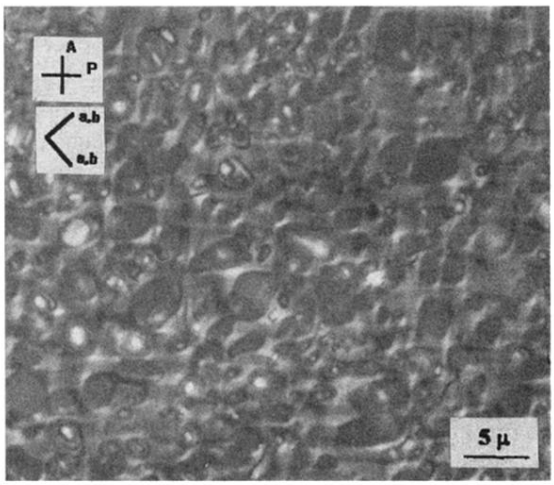

FIG. 9. Detwinning areas around small 211 particles.